Annual Progress Report 2, 2013-2014

NASA Award Number: NNX12AD28G

Global-scale assessment of threatened river delta systems: Evaluation of connections between the continental land mass and ocean through integrated remote sensing and process modeling.

City University of New York
Co-investigators: Charles J. Vörösmarty, Kyle McDonald, Balazs M. Fekete, Hansong Tang, Deborah Balk, Irina Gladkova, Michael Grossberg
Research Associate: Zachary D. Tessler
PhD Student: Hannah Aizenman

University of Colorado
Co-I: James P.M. Syvitski
Research Scientist: Albert J. Kettner
PhD Student: Stephanie Higgins
CSDMS, INSTAAR, Univ. of Colorado, 1560 30th St., Boulder CO, 80309
Award Number: PZ07124

1. Project overview

With population growth, development, and the specter of climate change-- sea level rise and changes in storm and flood surge exposure-- coastal wetland systems increasingly will become a major focal point of concern with respect to human vulnerability and sustainable development. The urgent need to study and develop a capacity to forecast the changing character of these linked geophysical-social systems serves as the chief impetus for our study. River deltas, in particular, are an important focal point for the impacts of humans on both terrestrial land mass and coastal zone systems, due to their position at the interface of these two major functional components of the Earth system. This project seeks to forward an integrated modeling and remote sensing system to assess their vulnerabilities by combining geophysical and social science perspectives. Our work is motivated by a major research challenge in the Earth system science: to identify, quantify, and understand how natural and human-dominated factors change freshwater discharge and riverborne sedimentary connections between the landmass and coastal ocean.

The overarching project **science goal** is "To analyze how the strength and variability of land-to-ocean links, as defined by riverine sediment fluxes, local anthropogenic activities and ocean processes, produce impacts on coastal delta systems, today and into the future."

Within this goal the University of Colorado worked on the following: 1) InSAR-derived subsidence maps, and 2) analysis of 8 years of 3 hourly ocean wave simulations.

The CUNY team's efforts during this year have focused on 1) further development of the land-ocean delta fingerprinting system, 2) improvements to WBM modeling of river networks in deltas, and 3) coastal ocean process modeling of sediment fates and remote sensing of sediment plume structure.

Several of the research topics discussed below were presented at an AGU Fall Meeting scientific session convened by Co-I's Syvitski and Vörösmarty entitled *"Deltas: A Multi-trillion Dollar Global Problem."* Additionally, a workshop proposal has been submitted to the "Deltas in Times of Climate Change II" International Conference in Rotterdam, The Netherlands, 24-26 September 2014, entitled *"Science-to-Action: Aligning science with stakeholder and community needs in the Mekong Delta system."* This session will provide an opportunity to share several of the data and modeling tools under development, and also obtain feedback from community and stakeholder leaders about how we can better bring our scientific efforts to bear on the challenges they face, particularly in the Mekong but in and other delta systems as well.

Major goals for the upcoming year focus on continuing to apply the context learned at the global and regional scales to the local delta scales. Specific plans include developing future scenarios of population growth and development in target Southeast Asia deltas (Mekong, Ganges, and possibly the Yellow), integrating these projections into current risk and vulnerability analyses, and prototyping a remotely sensed sedimentation analysis using *PALSAR* and *MODIS* for flood extent and *MODIS* and *LandSat* for estimated sediment load. This land-based product would complement and tie in to ongoing work in the upstream (*WBMsed* fluvial sediment transport model) and offshore domains (*ROMS+SWAN* coastal ocean sediment transport model) discussed below.

2. Research Progress 2013

2.1 InSAR-derived subsidence maps of target deltas [Stephanie Higgins, CU]

Interferometric Synthetic Aperture Radar (InSAR)-derived subsidence maps of the target deltas are a significant product of this project and are a key tool for assessing heterogeneities in space and time. In the previous annual report, we presented results from a submitted manuscript showing significant (> 12 cm/y) land subsidence at aquaculture facilities along the coast of the Yellow River Delta in China. Significantly, this work was the first to achieve direct measurements of aquaculture-induced land subsidence by any technique. Aquaculture facilities dominate large portions of most Asian megadeltas, but wet, muddy conditions have previously made both remote and *in situ* measurements challenging. Since the previous annual report, the article has been published [Higgins et al., *Geophysical Research Letters* 2013] (**Figure 1**), and the results have garnered significant attention; this work was featured by a descriptive article in Nature

(http://www.nature.com/news/fish-farms-cause-relative-sea-level-rise-1.13569) and widely reported by both national and international radio, online and print news outlets. Three presentations were made about this work at scientific conferences.

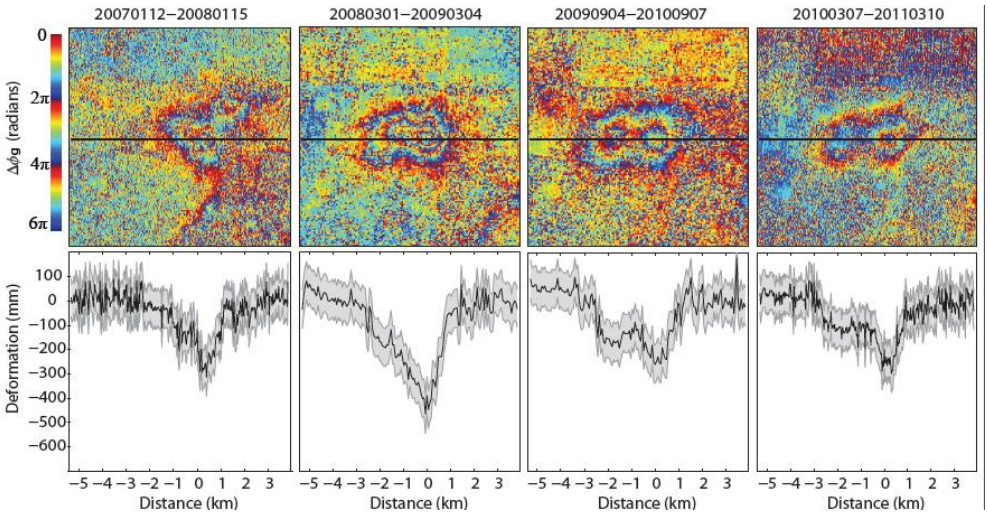

Figure 1: Example InSAR measurements over an aquaculture facility in the Yellow River Delta, China, showing a subsidence bowl in map view (top) and cross-section (bottom) over four years. Subsidence rates are as high as 30 cm/y at this subsidence "hot spot," the largest on the delta. From Higgins et al., [*GRL* 2013].

Over a second target delta, InSAR analysis is complete for a >10,000 km^2 portion of the Ganges-Brahmaputra Delta, Bangladesh (location, **Figure 2**). This work has been submitted for publication and is in review [Higgins et al., *Journal of Geophysical Research*, in review]. The study reconstructs subsidence rates in the most populous portion of the Ganges-Brahmaputra delta at a high spatial resolution of 90 m. Land subsidence of 0 to > 10 mm/y is seen in the capital city of Dhaka, likely related to groundwater extraction with rates corresponding to local variations in shallow subsurface sediment properties (**Figure 3**). Outside of the city, where abstraction is still high, rates vary from 0 to > 18 mm/y (**Figure 4**). Lowest rates appear primarily in Pleistocene clays and the highest rates in Holocene marshy clays and peat. Results demonstrate that subsidence in this delta is primarily controlled by local stratigraphy, with rates varying by more than an order of magnitude depending on soil properties.

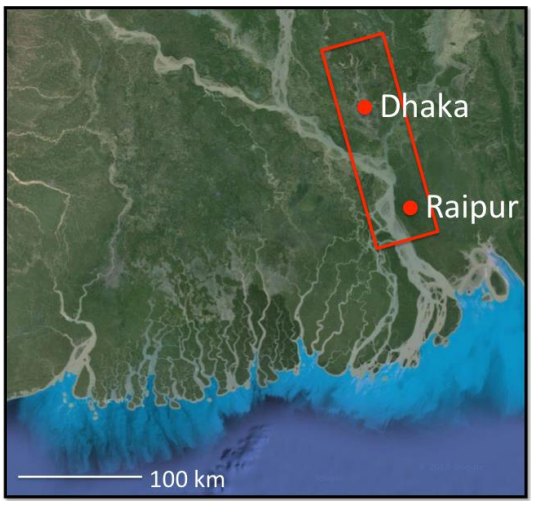

Figure 2: Location of InSAR study area in the Ganges Delta, Bangladesh.

These high-resolution subsidence maps provide important case-studies against which to test the global-scale fingerprinting method under development in this project. In the Ganges Delta, for instance, it is a combination of variable stratigraphy and local groundwater extraction rates that determine which parts of the delta experience subsidence rates of up to 2 cm/y. Even within the city of Dhaka, where

groundwater extraction is uniformly high, local stratigraphy controls compaction rates and therefore determines the change in elevation driven by human activities.

Towards Yr 3 goals for this project, SAR data has been acquired over the two more target deltas: the Indus delta in Pakistan and the Irrawaddy delta in Myanmar (Burma). A third manuscript is also in preparation describing the benefits and limitations of InSAR as a technique for generating subsidence maps in rural coastal settings. This work addresses the Yr 3 goal: *Papers and technical documentation, including methods of employing remote sensing for coastal ocean syndrome detection and analysis*, and aims to guide future work by providing direct processing chain improvements for InSAR analysis in these challenging settings.

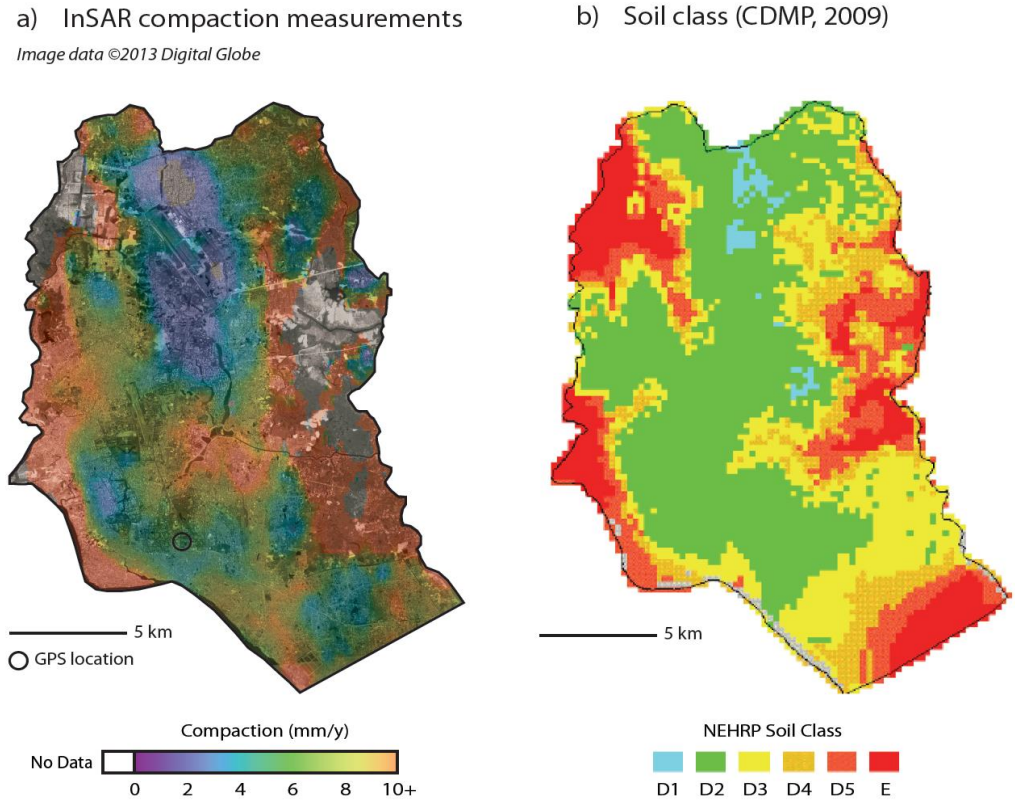

Figure 3: (a) InSAR-derived subsidence over the city of Dhaka, Bangladesh, 2007-2011. Boundaries are rivers bordering the city. (b) NEHRP soil classification, from stiffest (D1, blue) to loosest (E, red). Strong spatial correspondence suggests that groundwater extraction in the city is driving compaction of the loosest soils, while stiffer and older soils are stable despite rapid drawdown. From Higgins et al., [*submitted,* 2014].

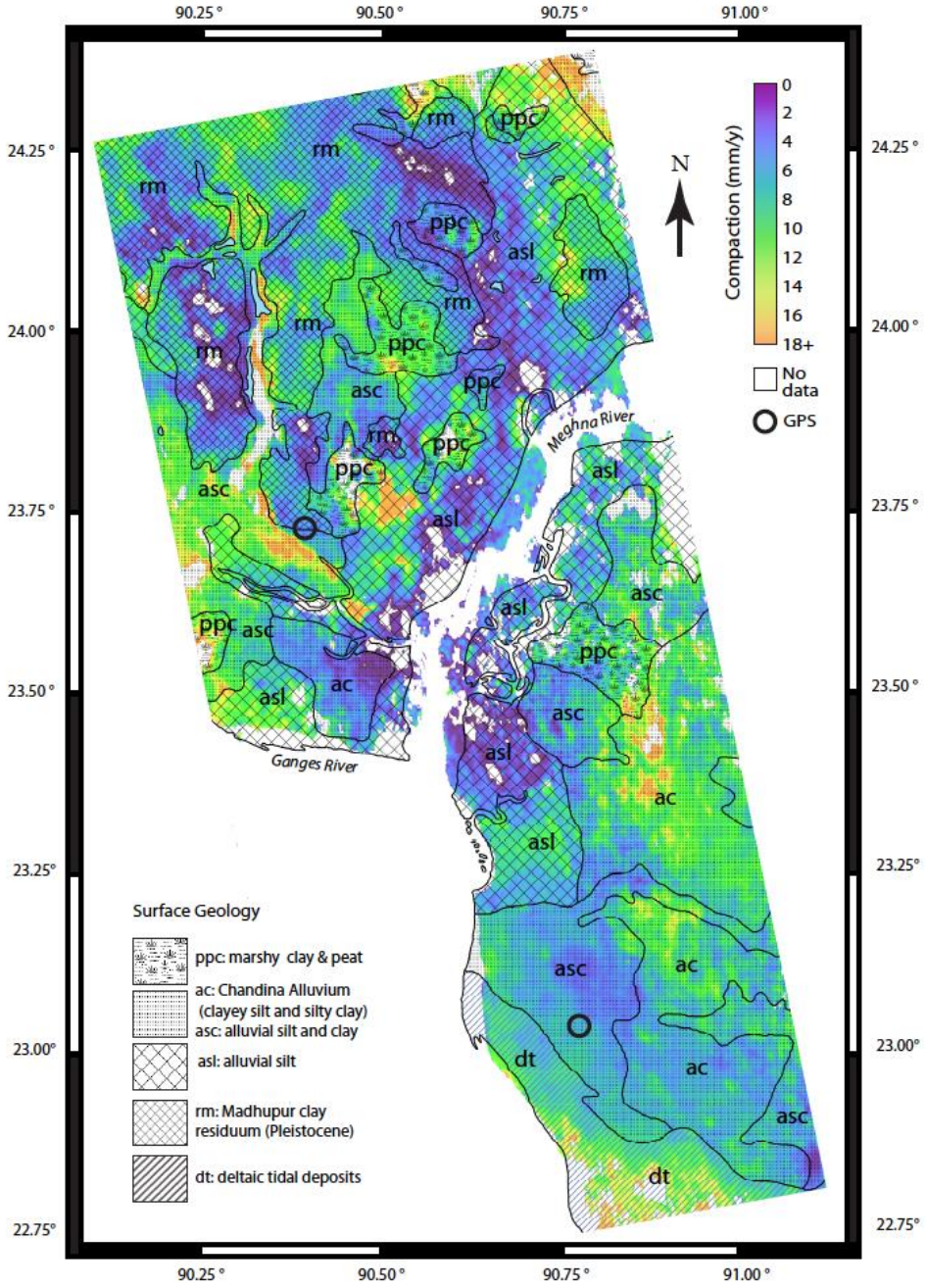

Figure 4: InSAR-derived average annual subsidence rates for a >10,000 km² section of the Ganges-Brahmaputra Delta, with surface geologic units from Geological Survey of Bangladesh [1998] superimposed. From Higgins et al. [*submitted,* 2014].

2.2 Analyses of ocean forcings on deltas [CU]

Ocean processes like waves and tides can have a profound impact on delta systems that partly determine a delta's morphology and its vulnerability. To study the impact of ocean processes on deltas, the results of an 8-year wave simulation (2005-2013) of WAVEWATCH III® are analyzed. The WAVEWATCH III® simulation was driven by the NCEP Climate Forecast System Reanalysis Reforecast (CFSRR) homogeneous data set of hourly 0.5° spatial resolution winds. Wave parameters (Table 1, spatial resolution 0.5°; temporal resolution: 3hour) were analyzed for the ocean domain grid cells directly adjoining the 5 deltas of interest of this study: Indus, Mekong, Ganges-Brahmaputra, Irrawaddy, Chao-Phraya.

Table 1. Each of the wave parameters that was analyzed

u	m/s	Wind speed 10m above MSL
v	degrees	Wind direction (were the wind is coming from) 10m above MSL
H	m	Overall significant wave height
T	s	Average peak period of the spectrum
dp	degrees	Average direction(were the wave are coming from) at peak period
p	kW/m	Average wave power, indirectly derived from *T* and *H*

Here, wave power is calculated determining the energy flux per unit of wave-crest length (eq. 1):

$$p = \frac{\rho g^2}{64\pi} H_{m0}^2 T \approx \left(0.5 \frac{kW}{m^3.s}\right) H_{m0}^2 T \qquad \text{(eq. 1)}$$

For the deltas of interest a frequency analysis for each of the wave parameters (Table 1) as well as analyses of large events was undertaken to be able to better understand the significance of waves on the deltas (section 2.2.1). Wave direction is in this regard of importance as waves towards land could make a delta more vulnerable than waves away from land. Additionally, wave parameter time series will be used in combination with simulated river flux (water and sediment discharge) time series to analyze if e.g. the timing of large riverine flux events corresponds to higher than average wave heights. Preliminary results for these event studies are presented in section 2.2.2.

2.2.1 Annual and seasonal wave frequency analysis

Eight years of 3 hourly data was analyzed to determine the annual and seasonal frequency distribution for each of the parameters for a given wave direction, see for example **Figure 5**.

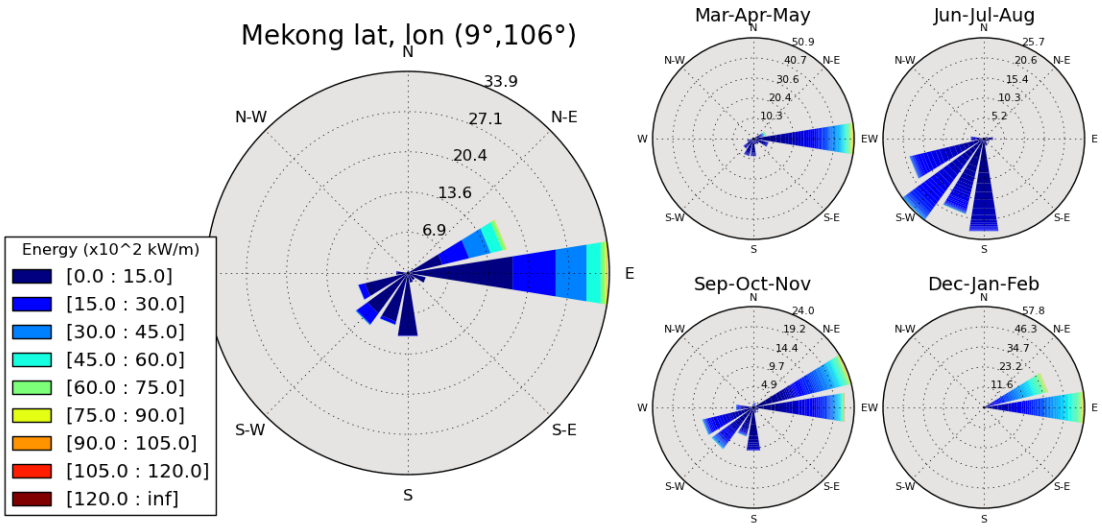

Figure 5. Annual and seasonal wave energy frequency distribution per wave direction for the Mekong Delta.

Based on this analysis, the deltas of interest can be ranked by their potential induced vulnerability due to wave energy, disregarding wave direction (Table 2).

Table 2. Wave energy per delta based on 8 year 3hourly WAVEWATCH III® *simulation*

Delta	**Average wave energy** (kW/m) *	**Maximum wave energy** (kW/m) *
Ganges-Brahmaputra	13,159	215,495
Indus	10,290	152,470
Irrawaddy	6,384	138,798
Mekong	1,397	12,125
Chao-Phraya	329	8,056

* Note: Wave direction is not taken into account

A more thorough wave analysis, including wave direction, is scheduled for year 3 of this project including a datasets that covers a larger period (30years vs. 8years). These results will be combined with the same 30year period of simulated riverine flux to analyze synchronicity versus a-synchronicity of peak terrestrial fluxes and peak wave energy in relation to delta flooding. Riverine fluxes are estimated as an effort of last project year, applying *WBMsed* (Cohen et al., 2014).

2.2.2 Large event wave analysis

Single large climatic events (e.g. tropical storm or a typhoon) can have a significant impact on the vulnerability of a delta. For each delta of interest a few tropical storms or typhoons were chosen that occurred within the time frame of the availability of

wave data (2005-2013) (**Figure 6**).

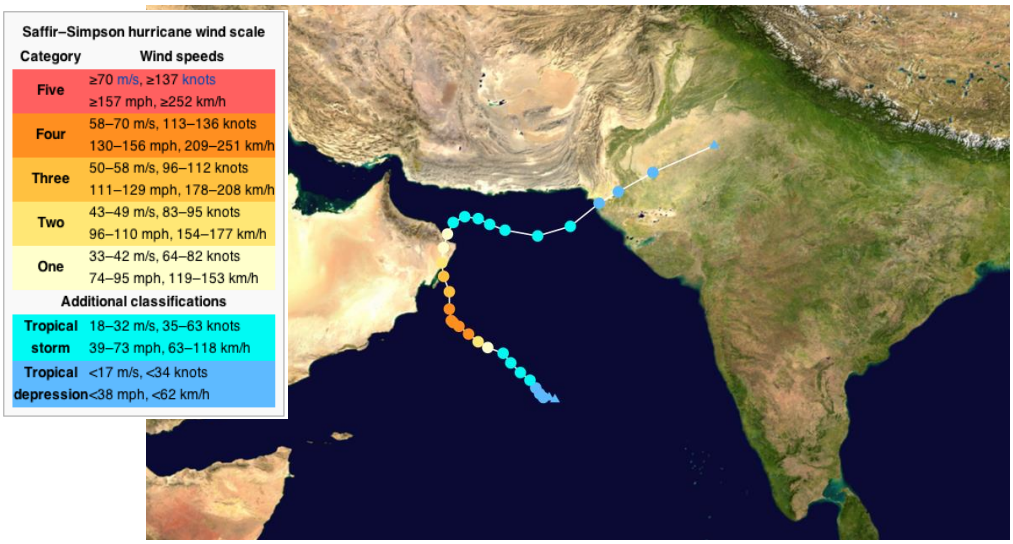

Figure 6. Example of a single large climatic event. The storm track of tropical storm Phet that made landfall on the Indus Delta at June 6th, 2010.

Wind magnitude and direction as well as significant wave height, wave direction, wave period and energy were derived from *WAVEWATCH III*® simulations for each climatic event. *WAVEWATCH III*® simulations are able to capture these large climatic events (**Figure 7**). As expected, the significant wave height and peak energy as well as the wave period all increase when Phet made landfall. Fluvial fluxes towards the delta (water discharge and suspended sediment load) are incorporated in Figure 7 as well to provide a visual comparison of the timing between ocean forcings and terrestrial fluxes towards the delta. Both water discharge and suspended sediment load increase during, but stay elevated after landfall of Phet. A more thorough wave – fluvial flux analysis is scheduled for year 3.

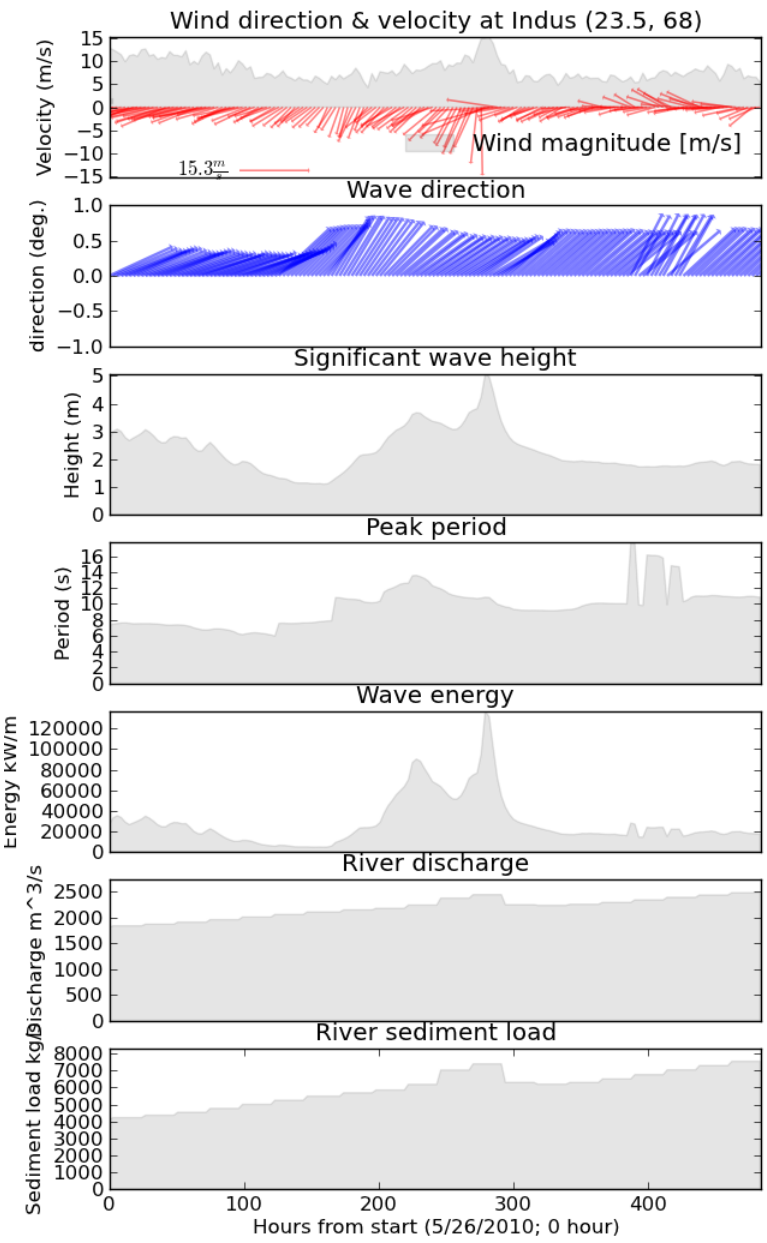

Figure 7. Wind, wave parameter characteristics (*WAVEWATCH III*®) as well as water discharge and sediment flux derived from the *WBMsed* model towards the delta before, during and shortly after tropical storm Phet.

2.3 Land-ocean delta fingerprinting system [CUNY]

2.3.1 Environmental stress index

We have built upon the integrated land-ocean data bank work in 2012 to develop a global delta "environmental stress" classification and index (*fingerprinting)* system. Important environmental variables in the local delta and upstream river basin domains that have been individually shown to influence long-term delta sustainability are incorporated into the geospatial database. This database is then used to cluster the deltas and identify common modes of environmental stress.

Upstream basin extents are based on the Simulated Topographical Network at 6 arc-minute resolution (STN06) digital river network. Delta extents are based on maps developed by Ericson et al. (2006), though work this year has extended the number of mapped deltas from 40 to 52, updated the coastline source from *GTOPO30* to the higher resolution SRTM, where available, and developed a suite maps incorporating buffer areas around the deltas at 5, 25, 50, and 100km. Variables incorporated into the fingerprinting system include:

- Basin population density, 2000
- Delta population density, 2000, with 25km buffer
- Basin reservoir sediment trapping
- Basin wetland disconnectivity
- Delta wetland disconnectivity
- Basin impervious surfaces
- Delta impervious surfaces
- Delta groundwater depletion

Population density is mapped using a 25km buffer around the deltas to incorporate the influence of major urban areas just outside the margin of the "delta proper." Economic and environmental activities in the marginal cities can have a large influence on the delta itself, even if the communities outside the delta are themselves less at risk of long-term subsidence and relative sea-level rise. The Mekong Delta is one example of a delta with a large urban population just outside the delta (**Figure 8**).

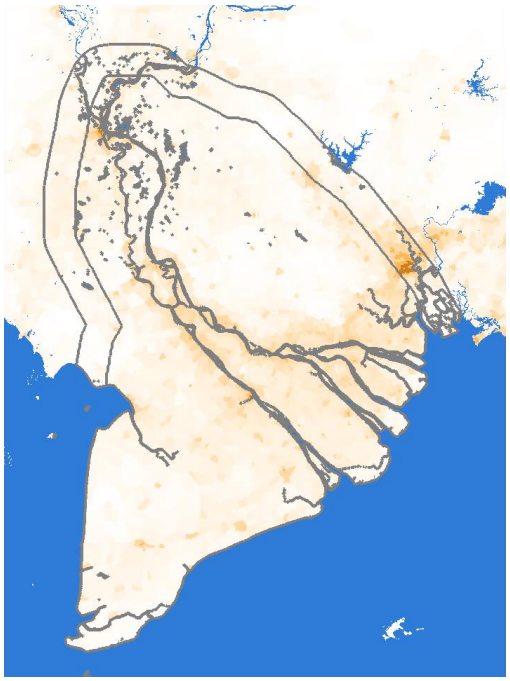

Figure 8: Mekong River Delta extent. Outer boundary is 25km buffer. Ho Chi Mihn City is within this buffer zone.

While there is some variation in the timestamp of each dataset, the datasets are all from the early 2000s. Work during the next year will extend the range of dates for possible comparison of delta trends. After extracting the mean of each variable over the delta or river basin extent, the data was rank-normalized across all deltas and clustered using an affinity propagation algorithm (**Figure 9**).

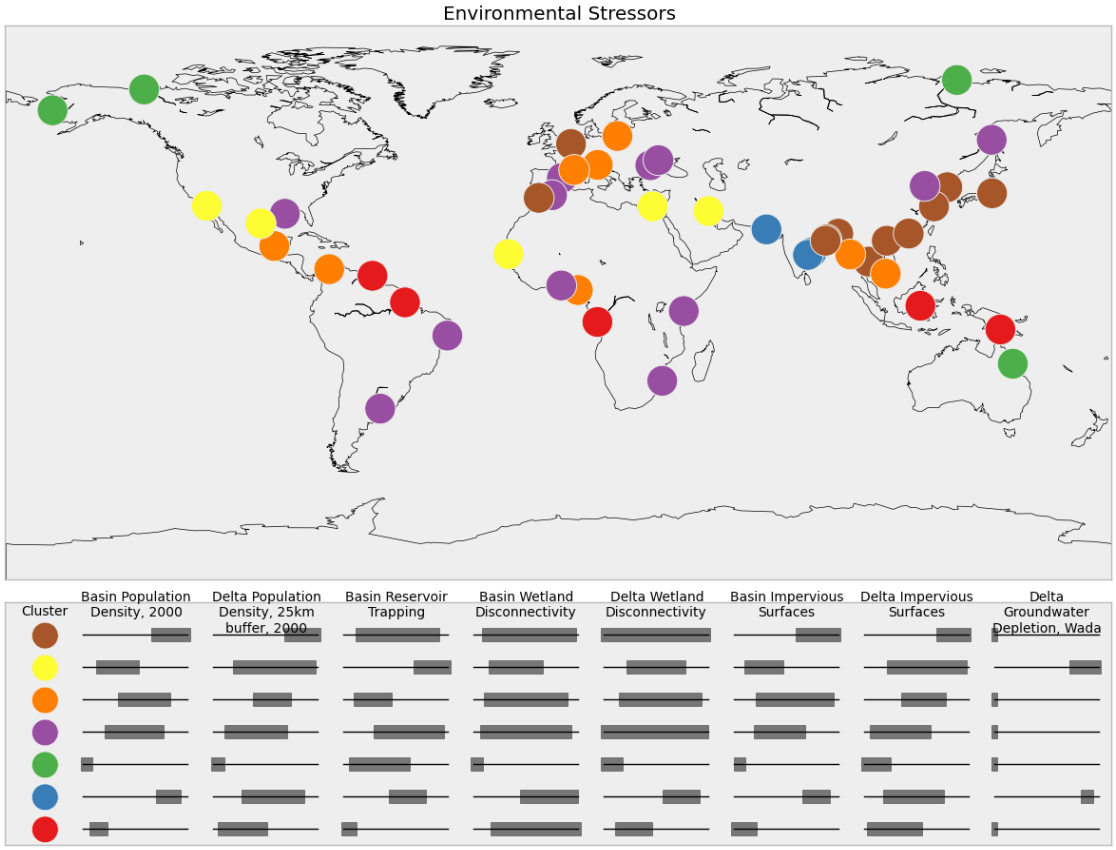

Figure 9: Delta clustering across the data bank of upstream and local delta stress variables. Colors indicate deltas with common patterns of environmental stress. The bottom panel indicates the rank-normalized range of the deltas in a particular cluster relative to all deltas, for each variable.

The clustering identifies several common modes (*syndromes)* of environmental stress. High latitude deltas, along with the Burdekin (cluster 2, **Figure 10**, left), are under relatively little environmental stress due to low populations and low development; upstream dams, while low, are the dominant source of stress. Cluster 5 (**Figure 10**, right) consists of moderately- to highly-stressed deltas, particularly related to water resources. The upstream basins are heavily dammed, and groundwater extraction in excess of recharge rates for agriculture is common. Cluster 6 deltas are predominately in Southeast Asia. These systems are heavily populated and urbanized both in the delta itself and the upstream basins.

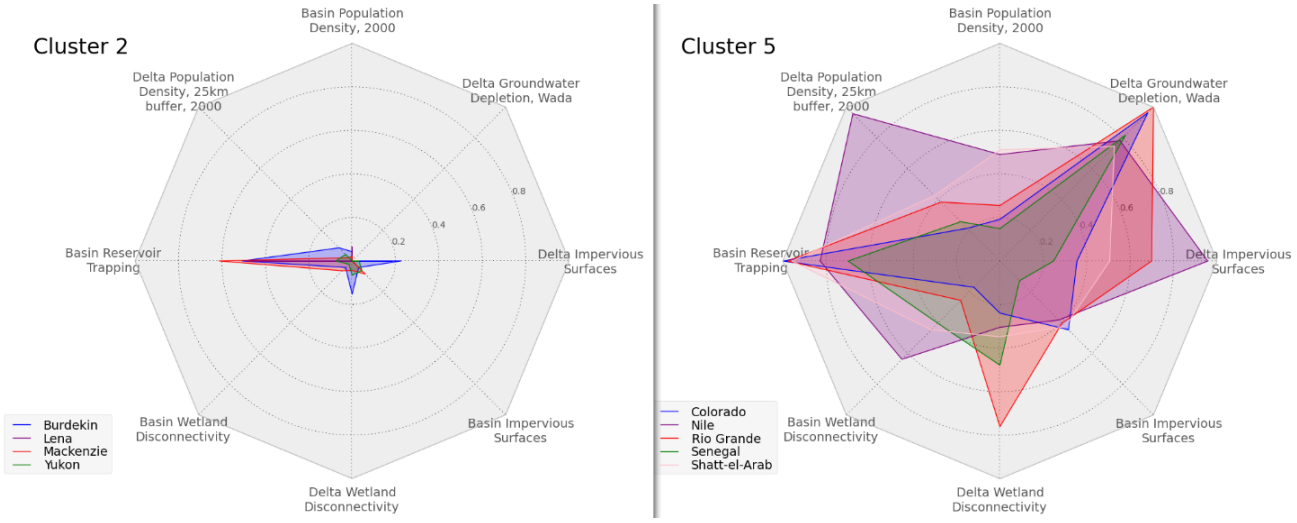

Figure 10: Delta clusters 2 (left) and 5 (right). Cluster 2 deltas are under low levels of environmental stress due to low populations and development on the delta. Upstream dams are the dominant source of stress. Cluster 5 deltas are moderately- to highly-stressed deltas are under heavy stress related to water resources. The upstream basins are heavily dammed, and groundwater extraction in excess of recharge rates for agriculture is common.

In addition to classification of each delta by common patterns, the integrated data bank has also been used to develop an environmental stress index. The main challenge in constructing this index is determining the proper relative weighting for the stress indicators. A first pass, using equal indicator weights, of our environmental stress index is in **Figure 11**.

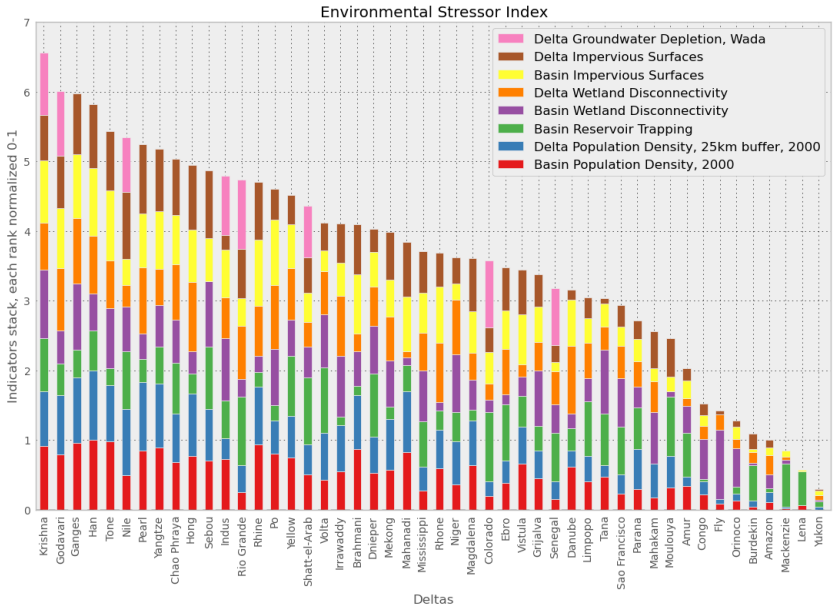

Figure 11: Environmental stress index constructed using constant weights across each indicator variable.

Deltas with high stress index values include the Krishna, Godavari, Ganges, Han, Tone, Nile, and Pearl. Low stress deltas include the four deltas in cluster 2 (Yukon,

Lena, Mackenzie, and Burdekin), as well as the Amazon, Orinoco, Fly, and Congo.

These index scores are dependent on the relative weighting of each indicator variable. While delta subsidence models can be used to directly compare the influence of some of these variables, incorporating the effect of imperious surfaces or wetland disconnectivity on subsidence is less clear. In order to explore the dependence of the delta stress index on indicator weights, we performed a sensitivity analysis by sampling the entire possible vector space of indicator weights. For each delta, we then calculated the distribution of possible index scores. Among 48 deltas, the RMS error between the equal weight index rank and the mean index rank was 3.11, suggesting that for most deltas, the equal weighting provides a reasonable estimate of the mean index score across all weights. For example, the Chao Phraya mean index score is 14.63, while using equal weights it has an index score of 11 (**Figure 12**, left). Deltas where the stress index is dominated by a few indicators, such as the Colorado, have a much larger stress index distribution as they are sensitive to the relative weight of those indicators (**Figure 12**, right).

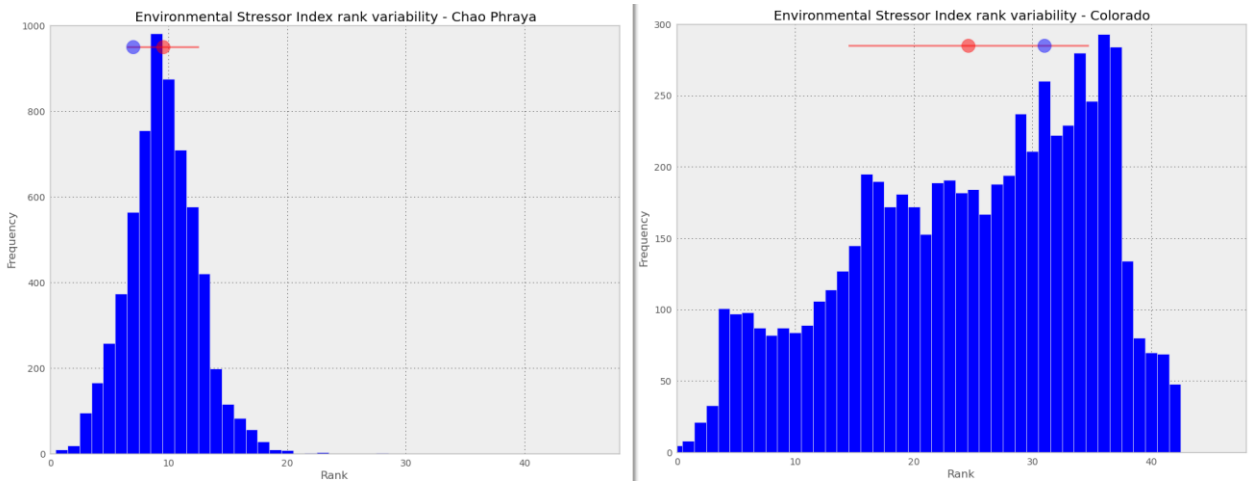

Figure 12: Chao Phraya (left) and Colorado (right) delta environmental stress index sensitivity to indicator weightings. The distribution of index scores is obtained by exploring the vector space of indicator weights. The red dot indicates the mean index score, while the blue is the score obtained from equal variable weights. The red bar width is the standard deviation. High ranks indicate greater environmental stress. The Colorado stress index is particularly sensitive to the weighting of the Reservoir Trapping and Groundwater indicators, resulting in a wide range of possible index scores as the weights are varied.

It is important to note that this environmental stress index is not a direct indication of delta risk or vulnerability. Rather, each indicator directly or indirectly represents a process that is driving changes in the upstream basin or at the local delta. These changes in turn affect the risk to the communities and ecosystems on the deltas. In this framework, these stresses are the driving forces that move a delta to a different state of vulnerability, acting through changes to the elevation, or destruction of protective wetlands for instance. One measure of future deltas at risk are those systems being driven to increased vulnerability, while also exposed to high hazards.

Work is ongoing to develop an index of delta hazards that, combined with the

environmental stress index, will be useful for identifying delta systems with increasing risk. A preliminary hazard index, constructed from an extreme river discharge index, sealevel rise trends, and cyclone risk is in **Figure 13**. Deltas that are under high stress and also are places exposed to high hydrological hazards include the Han, Pearl, Hong, Yangtze, Tone, Rio Grande, Godavari, Ganges, Chao Phraya, and Yellow deltas. The Nile, for instance, is a delta where stress levels are high, but background hydrological hazards are low, suggesting changes to future flood risk may be more moderate than expected from high environmental stress alone.

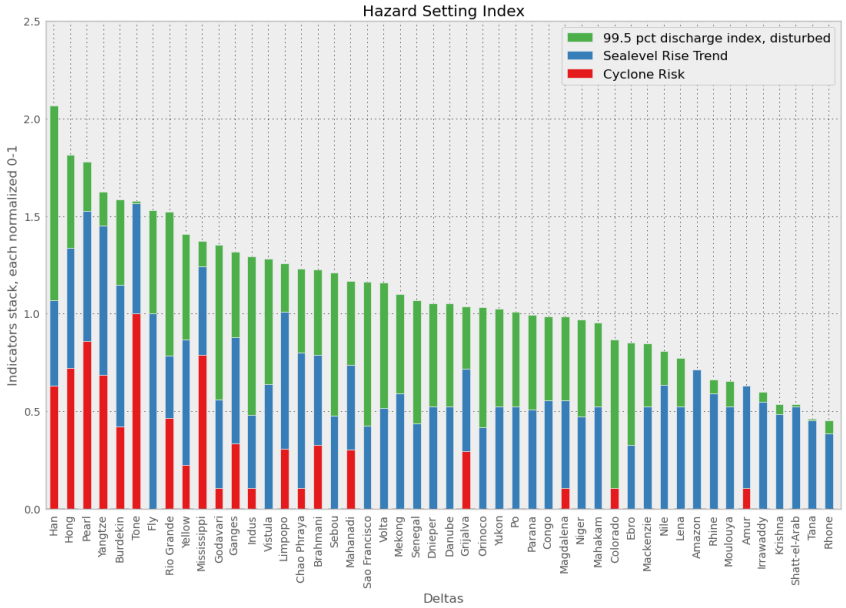

Figure 13: Hydrological hazard stress index constructed using constant weights across each indicator variable. This index is compared with the environmental stress index to identify deltas where were flood risk is likely to increase into the future.

2.3.2 Delta flood sensitivity

In addition to investigating background environmental stress, work is ongoing in the development of statistical tools to better quantify delta sensitivity to hydrological hazards. Using time series data from a number of sources, including *WAVEWATCH III* offshore waves, *WBM* river discharge and groundwater extraction, local precipitation, remotely sensed land surface inundation, and NDVI, we are looking for statistical relationships with flood state, as identified in the Dartmouth Flood Observatory database (**Figure 14**).

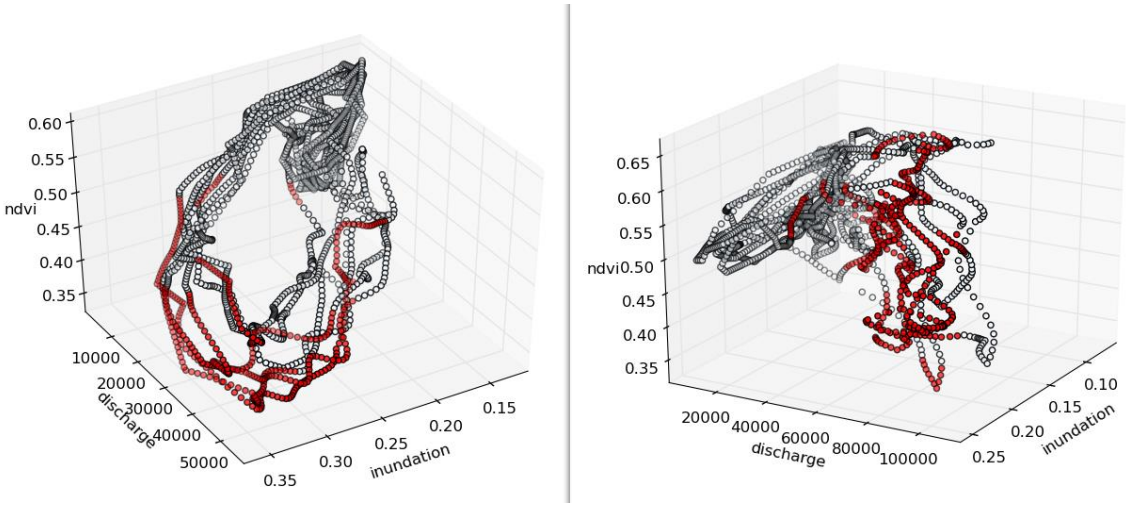

Figure 14: Scatter plots of delta-averaged NDVI, WBM river discharge, and delta-averaged land surface inundation fraction for the Mekong (left) and Ganges (right) deltas. Red dots indicate time periods identified as a flood in the Dartmouth Flood Observatory database.

Different deltas may experience similar discharge and inundation forcing, yet vastly different flood outcomes. In the Ganges for instance, discharge appears to be the most important variable for predicting flood state. In contrast, in the Mekong, high inundation and low NDVI appear to contain more information. Looking at the mean hydrological conditions during flood periods in the Mekong, we see several differences from the global "average" delta (**Figure 15**).

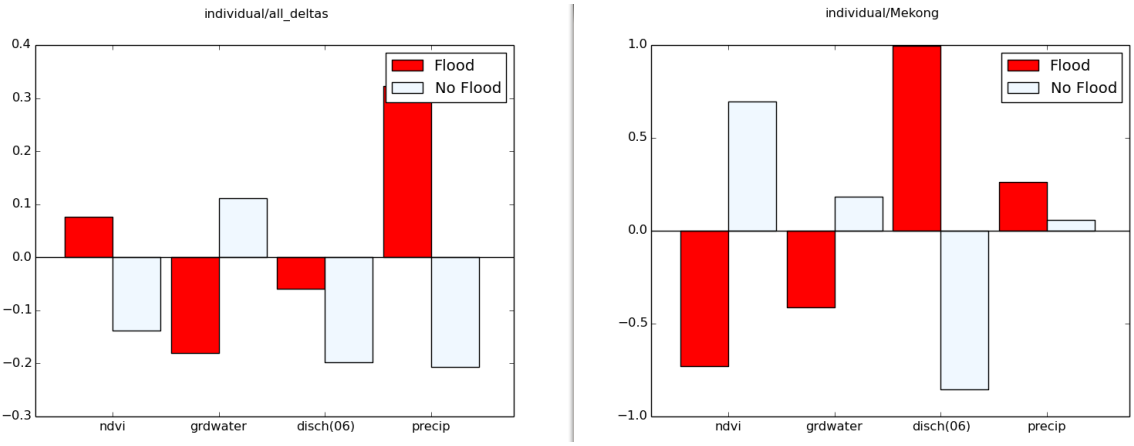

Figure 15: Hydrologic and vegetative conditions during flood and non-flood time periods, for all deltas (left) and the Mekong (right). Globally, flood state partitions the precipitation record into more distinctly different halves than the discharge. In contrast, Mekong flood state appears more related to river discharge. These data have been statistically resampled to balance the number of flood days with non-flood days.

In particular, flood-state partitions the precipitation record into distinctly different halves. In contrast, Mekong flood-state appears more strongly related to river discharge, suggesting the Mekong delta is less sensitive to local precipitation relative to other deltas. We are also investigating the use of several statistical classifiers on this dataset to better understand differences in the variable dynamics underlying delta flood occurrences. As an example, **Figure 16** shows results from a

Linear Discriminant Analysis classifier after projecting the NDVI, groundwater extraction, river discharge, and precipitation records onto the first two principal components. This classifier allows us to examine differences between conditions that are correctly and incorrectly identified as flood. In this case, conditions where PC1 is strongly negative (likely flood) or strongly positive (likely no flood) are more often classified correctly than at moderate values of PC1. This is consistent with **Figure 15**, as PC1 is strongly positive when NDVI and groundwater extraction are positive, and discharge is negative. Thus flood conditions are unlikely when groundwater is being used, or discharge is low, consistent with increased use of groundwater for agriculture during dry conditions.

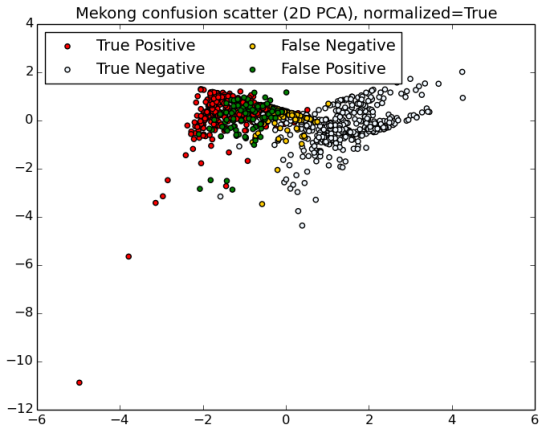

Figure 16: Confusion scatter plot of flood data classified by a linear discriminant analysis, for the Mekong delta. The first principal component is on the horizontal, the second on the vertical. The classifier performs best (red dots are true positives, white are true negatives) at low and high PC1 values. High PC1 corresponds to high NDVI, high groundwater extraction, and low river discharge.

2.4 WBM hydrological model improvements in delta river networks [CUNY]

Delta landscapes are characterized by low topographic relief and complex river bifurcation and branching patterns. *WBM*, and other, digital river networks are generated by routing water from high to low elevations. However, this method performs poorly in deltas, where extended region of low relief make determining a dominant flow direction difficult, particularly using globally-available DEMs with vertical uncertainties on the order of several meters. Bifurcations represent additional challenges.

Traditional D8 encoded gridded network (linking one of the eight adjacent neighboring grid cells as the flow direction downstream) lacks the capability of representing bifurcations of river deltas or braided streams. While the common encoding using exponents of two could allow assigning multiple flow directions to each grid cell, but additional information about the partitioning of the flow to different branches is still needed for implementing flow simulation. Furthermore, bifurcations break the convenient tree hierarchy of the connected grid cells, which otherwise provides the basis for efficient routing that can propagate excess water from headwater to basin outlets.

Instead of modifying the well established network structures, our team decided to find alternative solutions to represent bifurcations based on the flow routing capabilities developed for inter-basin transfers. Inter-basin transfers are currently implemented in our modeling framework as arbitrary linkages between pairs of grid cells enabling water transfers between branches of the same river basin or between entirely different basins. We will use the same capabilities by creating pairs of points linking grid cells in the mainstem to adjacent "headwater" grid cells in currently disconnected basins. Just like the inter-basin transfer pairs of points, the bifurcation pairs of point can carry a series of attributes allowing the parameterization of flow partitioning. We are in the process of developing bifurcation database for major deltaic river system that will enable us to better represent the flow dynamics.

In our modeling framework, flow routing currently relies on sorting the grid cells by basin ID and the number of grid cells upstream, allowing to execute the flow calculations at the headwater grid cells first and propagate downstream. The cell ids assigned to each grid cell after sorting can be used to distinguish linkages (either inter-basin transfer or bifurcations) that link a grid cell that are above or below in the cell hierarchy. Since bifurcations will divert water from larger basins to smaller basins, they will be dominantly represent linkage to grid cells that are calculated later in the computation sequence unless, the recipient river segments loop back to the same main channel. Distinguishing between river connections that link river segments to higher or lower segment in the grid cell hierarchy will have ramification for the implementation for the flow routing.

2.5 Coastal ocean sediment fates [CUNY]

2.5.1 Process modeling of the coastal ocean

We are developing a coupled ocean, wave, and sediment model application for several of our deltas-at-risk. Details of the fate of fluvial sediment in the coastal zone is important to understanding how deltas will respond to future environmental forcings. We have begun developing models of two deltas, the Mekong and the Chao Phraya. Validation of the models is difficult without contemporary *in situ* observations, though we are leveraging satellite assets for preliminary analysis.

We are using the Regional Ocean Modeling System (*ROMS*), coupled to the wave model *SWAN*, with an integrated sediment transport model. For the Mekong simulation, our model is 160x128 grid cells, with a horizontal resolution of approximately 2km. There are 10 levels in the vertical that vary with total depth. Coastal bathymetry is interpolated from GEBCO, with some horizontal smoothing to increase model stability. The model is initialized and forced on the boundary by output from a global *HYCOM 1/12* degree model simulation. Surface forcing is based on the ERA Interim Reanalysis data set. Waves are forced on the boundary from the NOAA *WAVEWATCH III* global historical simulation output. Four tidal components (M2, S2, K1, O1) are extracted from the OSU *TPXO7.2* tidal inversion and

implemented in the model as a boundary forcing. Currently, the simulation time window is Jan-Dec 2006, though we anticipate extending this range.

Sediment is delivered to the coastal zone from 13 rivers, each spread over 3 grid points (**Figure 17**).

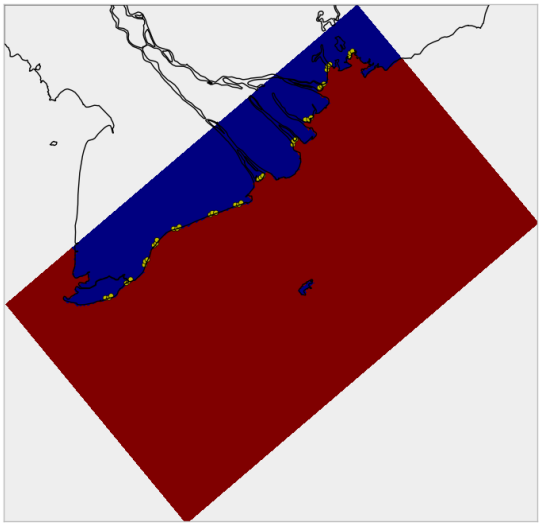

Figure 17: Mekong coastal model region, yellow dots indicate locations of river input.

These 13 rivers map to 2 *WBM* simulated rivers, whose discharge is distributed among the modeled river mouths. Currently, this distribution is handled in an ad-hoc manner, though with planned improvements to WBM river bifurcation handling, we expect to more directly simulate distinct river mouth discharge within the delta. For testing purposes, sediment concentrations output from these rivers are set to a constant (Syvitski and Milliman, 2007), though we intend to use *WBMsed* simulated sediment fluxes. Sediment grain properties are based on work by Xue et al. (2012). We use two sediment classes, a fine sediment class of 2 μm diameter that remain as single grains, and a 100 μm sediment class to represent flocculated muds. The flocculation process itself is not included in the model. The relative proportion of these sediments in the river input is constant, 30% fine single-grained sediment, 70% flocculated sediment. The model is initialized with no sediment on the seafloor, and zero sediment coming in from the boundaries.

Figure 18 (top row) shows preliminary simulation results for surface sediment and currents.

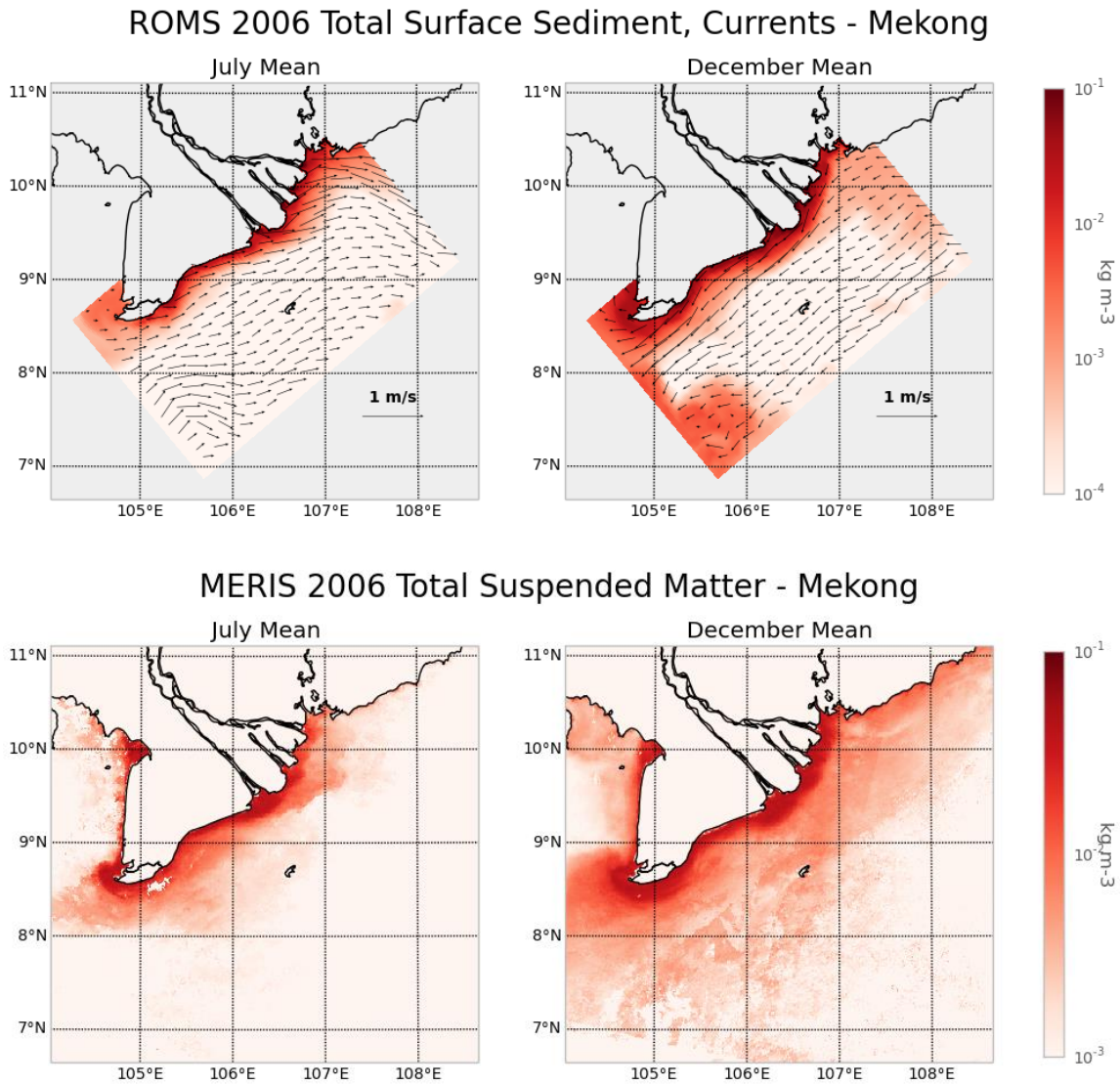

Figure 18: (Top row): Total surface sediment concentrations and surface currents at the Mekong river mouth, modeled, during July (top left) and December (right), 2006. Bottom row: Total Suspended Matter monthly means from constructed from all available *MERIS* swath images. Note difference in color bar range, background modeled sediment concentrations are roughly an order of magnitude lower than the *MERIS* product data.

Model results indicate that the majority of sediment is being retained close to shore, near the delta front. During the summer, currents draw sediment from the river mouths to the north and east. In contrast, in December the southwesterly currents transport sediment along the coast, and begin to wrap around the delta edge. The increased surface sediment in the southern-most portion of the grid during December may be an artifact of the open boundary conditions, which will be investigated. Our Chao Phraya model is configured similarly. Modeled surface sediment is shown in **Figure 19** (top row).

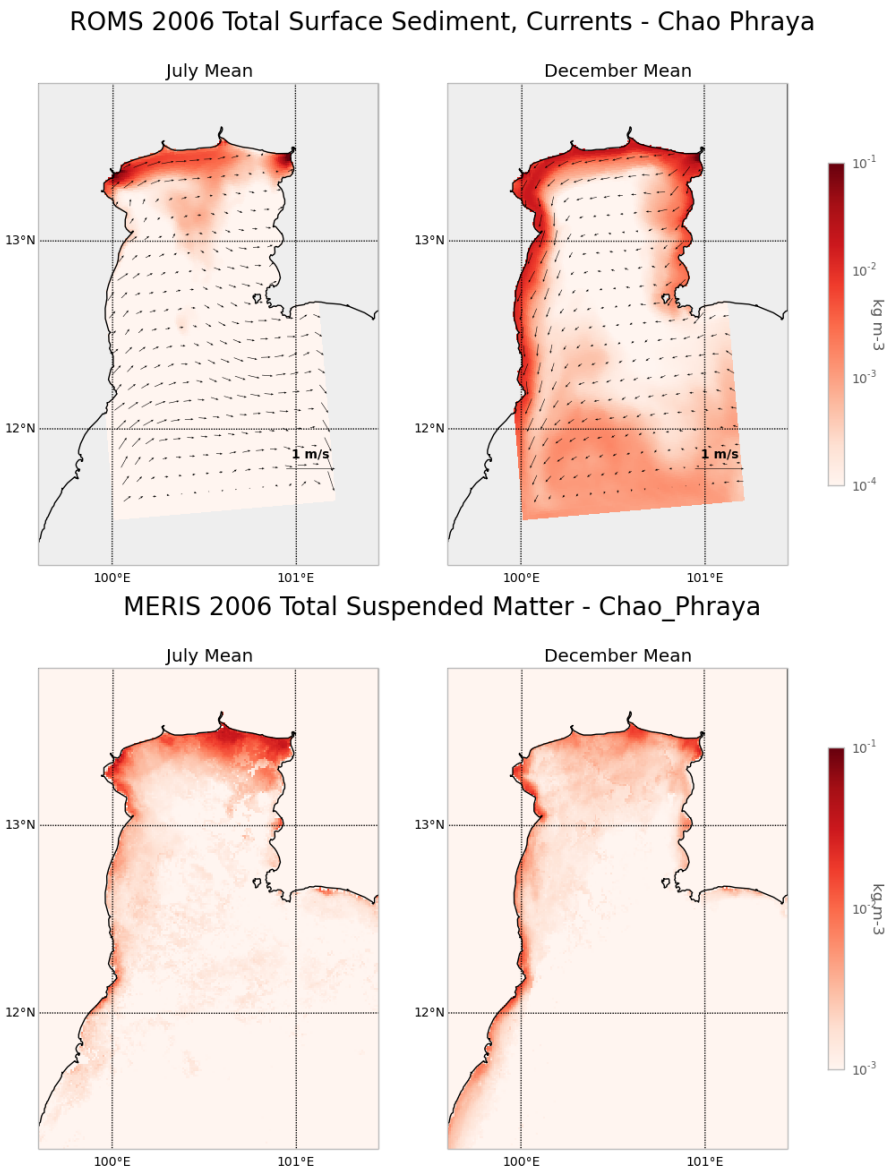

Figure 19: (Top row): Total surface sediment concentrations and surface currents at the Chao Phraya river mouth, modeled, during July (top left) and December (right), 2006. Bottom row: Total Suspended Matter monthly means from constructed from all available *MERIS* swath images. Note difference in color bar range, off-shore modeled sediment concentrations are roughly an order of magnitude lower than the *MERIS* product data.

2.5.2 Model validation with MERIS sediment plumes

As a basic model validation, we can compare the modeled surface sediment concentrations to remote sensing observations. We use the *MERIS* Level 2 Reduced Resolution Total Suspended product, which has a resolution of approximately 1km^2. All available *MERIS* data over the model grid during the year 2006 were used to generate the July and December monthly mean suspended matter images in **Figures 18** (Mekong, bottom pane) and **19** (Chao Phraya, bottom pane). All clear-sky ocean pixels for each month were averaged to construct the monthly means.

The Mekong *MERIS* data confirms the model finding that the majority of Mekong River sediment remains close to shore. During July, relatively more of the sediment plume is observed to the north east of the river mouth, while during December the plume more strongly extends down and around the south west delta edge, consistent with modeling results. Background sediment concentrations off shore are roughly an order of magnitude lower in the model. This may be due to initialization of the model with zero background sediment in the water column, and zero sediment on the sea bed. Model experiments will be conducted to see how a more realistic initialization state and sediment boundary condition affect the background sediment concentrations.

The Chao Phraya model appears to agree less well with observations that the Mekong model. The observations do show a slightly more intense sediment plume along the western boundary during December than during July, though the modeled results show this feature much more strongly. Additionally, modeled fluvial sediment outflow at the river mouths appears misallocated between mouths. *WBM* improvements to delta river network handling discussed above may help here.

Planned work over the next year is to use these coastal models to investigate how environmental changes to upstream (dam construction, decommissioning) and subaerial delta processes (river diversions, wetland loss) may impact the fate of sediment delivered to and deposited on the subaqueous delta. This work will entail data handoffs between *WBMsed* and the coupled *ROMS+SWAN* models described here, as well as the introduction of simple conceptual models delta processes. These will be implemented as modification in time, space, and sediment fluxes magnitude between *WBMsed* output and the coastal model input.

3. Publications & presented abstracts for project year 2013

Publications

Cohen, S., Kettner, A.J., and Syvitski, J.P.M., (accepted 2014). Global Suspended Sediment and Water Discharge Dynamics Between 1960-2010 based on the WBMsed v.2.0 Model. *Global and Planetary Change.*

Haddeland, I., Heinke, J., Biemans, H., Eisner, S., Florke, M., Hanasaki, N., Konzmann, M., Ludwig, F., Masaki, Y., Schewe, J., Stacke, T., Tessler, Z.D., Wada, Y., Wisser, D. (2013). Global water resources affected by human interventions and climate change. *Proceedings of the National Academy of Sciences*., doi: 10.1073/pnas.1222475110.

Higgins, S., Overeem, I., Tanaka, A. & Syvitski, J.P.M., (2013), Land subsidence at Aquaculture Facilities in the Yellow River Delta, China, *Geophys. Res. Lett.* 40(15), 3898-3902.

Higgins, S., Overeem, I., Steckler, M. & Syvitski, J.P.M., (2014), InSAR measurements of compaction and subsidence in the Ganges-Brahmaputra delta, Bangladesh, *J. Geophys. Res*., in review.

Overeem, I., Kettner, A.J., and Syvitski, J.P.M., 2013. Impacts of Humans on River Fluxes and Morphology, In: Editor-in-Chief: John F. Shroder, *Treatise on Geomorphology*, Volume 9: Fluvial Geomorphology, Academic Press, San Diego, Pages 828-842.

Syvitski, J.P.M., Kettner, A.J., Overeem, I., Giosan, L., Brakenridge, G.R., Hannon, M., and Bilham, R., (submitted 2013). The Indus Delta and its Sindh Floodplain: a Holocene to Anthropocene Transition. *The Anthropocene*.

Syvitski, J.P.M., Cohen, S., Kettner, A.J., and Brakenridge, G.R., (accepted 2013). How important and Different are Tropical Rivers? – An overview. *Geomorphology*.

Tang, H.S., Chien, S. I-Jy, Temimi, M., Ke, Q., Zhao, L.H., Blain, C.A., Kraatz, S. Vulnerability of population and transportation systems at east bank of Delaware Bay to coastal flooding in climate change conditions. Natural Hazards, 69(2013), 141-163.

Wada, Y., Wisser, D., Eisner, S., Florke, M., Gerten, D., Haddeland, I., Hanasaki, N., Masaki, Y., Stacke, T., Tessler, Z., and Schewe, J. (2013). Multi-model projections and uncertainties of irrigation water demand under climate change. *Geophysical Research Letters*, 40, 4626-4623.

Presentations

Ashton, A.D., Nienhuis, J., Ortiz, A.C., Trueba, J.L., Giosan, L., Kettner, A.J., Xing, F., December, 9-13th, 2013. Effects of marine reworking and sea-level rise on deltas of the 21st century, *AGU*, San Francisco, CA, USA.

Cohen, S., Kettner, A.J., Syvitski, J.P.M., April 14-17, 2013. Human and climate impact on global riverine water and sediment fluxes - a distributed analysis. *American Geophysical Union (AGU Meeting of the Americas)*, Cancun, Mexico.

Cohen, S., Kettner, A.J., Syvitski, J.P.M., December, 9-13th, 2013. Anthropogenic effects on global riverine sediment and water discharge - a spatially explicit analysis, *AGU*, San Francisco, CA, USA.

Higgins, S., Overeem, I., Tanaka, A., & Syvitski, J. P. M., (2013), Land Subsidence at Aquaculture Facilities in the Yellow River Delta, China, *Annual Meeting of the American Geological Society (AGU)*, San Francisco, CA, Dec 9 – 12, 2013.

Higgins, S. & Syvitski, J. P. M., (2013), Land Subsidence at Aquaculture Facilities in the Yellow River Delta, China, *1st Annual Workshop on Coastal Subsidence,* New Orleans, LA, Nov 19 – 21, 2013.

Higgins, S., Overeem, I., & Syvitski, J. P.M., (2013), Fish Farms and the Sinking Delta, *Community Surface Dynamics Modeling System (CSDMS) 2.0: Moving Forward*, Boulder, CO, Mar 23 – 25, 2013.

Kettner, A.J., Syvitski, J.P.M., Overeem, I., Brakenridge, G.R., December 9-13th, 2013. Fluvial geomorphological changes of the Indus River due to human failure, *AGU*, San Francisco, CA, USA.

Kettner, A.J., August 28-30th, 2013. Advances in simulating fluvial sediment transport at basin-scale. *Stratodynamics*, Nagasaki, Japan.

McDonald, K., Chapman, B., Schroeder, R., Azarderakhsh, M., Podest, E., Moghaddam, M., Whitcomb, J., Hess, L., Kimball, J. (2013) Assembly and Assessment of ASCAT Scatterometer Data for Continuing Global Vegetation State Monitoring: Comparison with SeaWinds-on-QuikSCAT and Vegetation Response to Seasonal Drought, 2013 NASA Terrestrial Ecology Science Team Meeting, Scripps Seaside Forum, La Jolla, CA, USA.

Schroeder, R., McDonald, K.C., Azarderakhsh, M., Steiner, N., Dunbar, R.S., Zimmermann, R., Küppers, M. December 9-13th, 2013. ASCAT MetOp-A Backscatter Observations over the Global Land Surface: Application to Monitoring Recent Trends in Lake and Wetland Extent and to Monitoring Crop Growth over the United States, *AGU*, San Francisco, CA, USA.

Slayback, D., Policelli, F.S., Brakenridge, G.R., Tokay, M.M., Smith, M.M., Kettner, A.J., December 9-13th, 2013. Global, Daily, Near Real-Time Satellite-based Flood Monitoring and Product Dissemination, AGU, San Francisco, CA, USA.

Syvitski, J.P.M., Cohen, S., Kettner, A.J., Brakenridge, G.R., December 9-13th, 2013. New Possibilities in Global Hydrology and Sediment Transport, *AGU*, San Francisco, CA, USA.

Tessler, Z.D., Vörösmarty, C.J., June 5-6, 2013. Environmental stress and relative sea level rise in river delta systems, *NOAA-CREST Symposium: Climate and Extreme Weather Impacts on Urban Coastal Communities*, New York, NY, USA.

Tessler, Z.D., Vörösmarty, C.J., December 9-13, 2013. A global deltas typology of environmental stress and its relation to terrestrial hydrology, *AGU,* San Fransisco, CA, USA.

Vörösmarty, C.J, Foufoula-Georgiou, E., Tessler, Z.D., Overeem, I. January 9, 2014. Environmental CrossRoads and a New Global DELTAS Sustainability Initiative. Deltares, Rotterdam, The Netherlands.